A Ship-in-a-bottle Strategy to Synthesize Encapsulated Intermetallic Nanoparticles: Green Catalysts for Furfural Hydrogenation

Raghu V. Maligal-Ganesh,[†] Chaoxian Xiao,[†] Tian Wei Goh,[†] Linlin Wang,[‡] Jeffrey Gustafson,[†] Yuchen Pei,[†] Zhiyuan Qi,[†] Duane Johnson,[‡,§] Shiran Zhang,[#] Franklin (Feng) Tao,[#] and Wenyu Huang[*, †, ‡]

[†]Department of Chemistry, Iowa State University, Ames, Iowa 50011, United States

[‡]Ames Laboratory, U.S. Department of Energy, Ames, Iowa 50011, United States

[§]Department of Materials Science and Engineering, Iowa State University, Ames, IA 50011 (USA)

[#]Department of Chemical & Petroleum Engineering, Department of Chemistry, University of Kansas, Lawrence, KS 66045

KEYWORDS: Intermetallic compounds, site isolation, heterogeneous catalysis, core-shell, ship-in-a-bottle.

ABSTRACT: Intermetallic compounds are garnering much attention to their prowess as efficient catalysts for improved selectivity in chemical processes. Herein, single phase platinum containing intermetallic nanoparticles (NPs) protected by a mesoporous silica ($mSiO_2$) shell were synthesized by the heterogeneous reduction and nucleation of Sn, Pb, or Zn on $mSiO_2$-encapsulated Pt NPs using a *ship-in-a-bottle* strategy. In the selective hydrogenation of furfural to furfuryl alcohol, a dramatic increase in activity and selectivity was observed when the intermetallic NPs were used as the catalyst in comparison to $Pt@mSiO_2$. Among the intermetallic NPs, $PtSn@mSiO_2$ exhibited the best performance, requiring only one-tenth of the quantity of Pt used in $Pt@mSiO_2$ for similar activity and close to 100% selectivity to furfuryl alcohol. Carbon deposition-induced catalyst deactivation could be conveniently reversed via a high-temperature oxidation-reduction treatment. XPS measurements further shed light on the relevance of surface composition to the activity. Using density functional theory (DFT) calculations, the enhanced selectivity to furfuryl alcohol on PtSn in comparison with Pt was attributed to the different adsorption configurations of furfural on these two surfaces.

■ INTRODUCTION

Intermetallic compounds have been the subject of significant scientific interest as efficient catalytic materials with vastly improved activity and selectivity compared to their monometallic counterparts.[1-4] The site isolation of the active metal in these ordered structures, as opposed to their random arrangement in alloys, affords geometric and electronic changes directed towards noticeable enhancement in activity, selectivity and stability during catalysis.[5] The synthesis of these intermetallic compounds however involves high temperatures and an inability to exert control over size or morphology, resulting in lower surface areas for catalysis.

Nanosizing intermetallic compounds to increase their specific surface areas is necessary to increase their activity by several orders of magnitude.[6,7] Schaak et al. reported the synthesis of a number of nanocrystalline intermetallic compounds using low-temperature solution chemistry methods.[8-11] The use of organic stabilizers in their synthetic protocol provides limited protection against aggregation of the nanoparticles (NPs).[8,12] Furthermore, the use of popular supports (e.g., alumina and ceria) for the intermetallic NPs did not prevent aggregation completely.[13] A layered double hydroxide (LDHs) approach to obtain monodisperse nanoscale Ni-In intermetallic compounds for the enhanced chemoselective hydrogenation of α,β-unsaturated aldehydes has been reported.[14] Without the incorporation of Al or Mg in the Ni-In LDHs, however, severe aggregation was observed in the intermetallics during their synthesis.

In this work we report a unique and facile approach to synthesizing monodisperse nanoscale intermetallic compounds via seed NPs confined in a thermally robust inorganic capsule. Metal NPs encapsulated by inorganic shells have demonstrated enhanced stability at high temperatures compared to those capped with organic agents.[15-18] Pt NPs encapsulated in mesoporous silica shells ($Pt@mSiO_2$) demonstrated their stability against aggregation when annealed at 750°C.[19] Using the aforementioned $Pt@mSiO_2$ as the Pt seeds and the metal precursor of the additional metal (salts of Sn, Pb, Zn), we synthesized intermetallic compound NPs within the $mSiO_2$ shell. Low temperature solution chemistry methods[20,21] facilitated this *ship-in-a-bottle* conversion of $Pt@mSiO_2$ to the Pt-based intermetallic NPs as shown by the scheme in Figure 1. Intermetallic NPs synthesized by this method were well confined within the mesoporous silica environment. Moreover, the mesoporous silica encapsulation did not pose any hindrance during catalytic reactions.

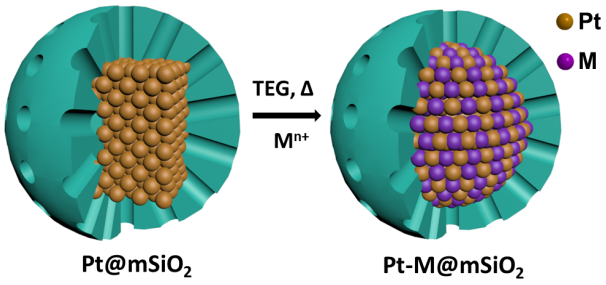

Figure 1: The ship-in-a-bottle synthesis of intermetallic NPs using a mesoporous silica-shell as a "nanoreactor", along with a solvent/reducing agent. The metal precursor (M^{n+}) corresponds to the particular metal salt added to obtain the intermetallic NPs, e.g. using Sn^{2+} to obtain PtSn or Pt_3Sn. We used tetraethylene glycol (TEG) for all but Pt-Zn, which used an oleyl amine/oleic acid mixture.

We chose the hydrogenation of furfural to demonstrate the catalytic property of the Pt-based intermetallic compounds. Upon hydrogenation, furfural (2-furfuraldehyde), an important renewable chemical feedstock,[22-24] produces furfuryl alcohol among other derivatives. Furfuryl alcohol features prominently as an important precursor in the synthesis of a wide variety of chemicals.[25-28] However, selectively hydrogenating furfural to furfuryl alcohol poses a considerable challenge.

Industrially, the toxic copper-chromite catalyst has been used to carry out vapor phase selective hydrogenation of furfural to furfuryl alcohol with moderate yields. However, significant deactivation of the catalyst occurs due to coking and the migration of chromium on the catalyst, effectively blocking the active sites on reduced copper NPs.[29] Additionally, the catalyst poses an environmental (toxic chromium) hazard, and reinforces the need to find greener alternatives. Using noble metal nanoparticle catalysts, the selectivity to furfuryl alcohol is poor with the increased possibility for decarbonylation and ring hydrogenation, as opposed to the selective hydrogenation of the carbonyl bond to obtain furfuryl alcohol.[30] Variations in shape, size, the use of supports and surface modifiers have been reported for improved selectivity.[31-35] However, these still require delicate methodologies and careful design, narrowing the possibility to recycle the catalysts in their optimum state.

Using Pd NPs capped with self-assembled molecules, selectivity to furfuryl alcohol could be controlled by blocking active sites responsible for the undesired reactions.[31] However, there is no enhancement in the activity of these catalysts to the desired product. On the contrary, the intermetallic compounds synthesized using the shape-in-a-bottle approach, especially $PtSn@mSiO_2$, activity was enhanced by ten-fold in comparison with $Pt@mSiO_2$ at nearly 100% selectivity to furfuryl alcohol. An additional advantage of the $mSiO_2$ protection is that a deactivated $PtSn@mSiO_2$ catalyst can be regenerated with a convenient oxidation/reduction treatment. We didn't observe any loss in activity and selectivity of the catalyst after six cycles of the regeneration treatment.

Results and Discussion

NiAs-type PtSn and PtPb intermetallic NPs were readily synthesized in tetraethylene glycol (TEG) and did not require further thermal treatment. PXRD of samples taken out at different times during synthesis of PtSn NPs indicated the formation of the intermetallic phase after 2 hours at 280°C (Figure S1). Cu_3Au-type Pt_3Sn NPs (Pt:Sn molar ratio = 3:1) were not formed in TEG, yielding alloy NPs instead. However, further annealing the alloy NPs at 600°C resulted in the ordered intermetallic Pt_3Sn NPs (Figure 2 and S13b).

Similarly, Cu_3Au-type Pt_3Zn and CuAu-type PtZn (1:1 molar ratio) were not obtained after the 350°C reaction in the mixture of oleyl amine and oleic acid until a further annealing treatement at 600°C under 10% H_2 in Ar. Further synthetic details can be found in the Materials and Methods section in the supporting information. Powder X-ray diffraction (PXRD) patterns (Figure 2) confirmed the formation of the intermetallic phases of Pt_3Sn, PtSn, Pt_3Zn, PtZn, and PtPb, when compared to their corresponding simulated patterns.

Transmission Electron Microscopy (TEM) images confirm that the intermetallic NPs are monodisperse and encapsulated within the mesoporous silica shell after the synthesis (Figure 3), which indicates the secondary metal deposits on the Pt core in $Pt@mSiO_2$.

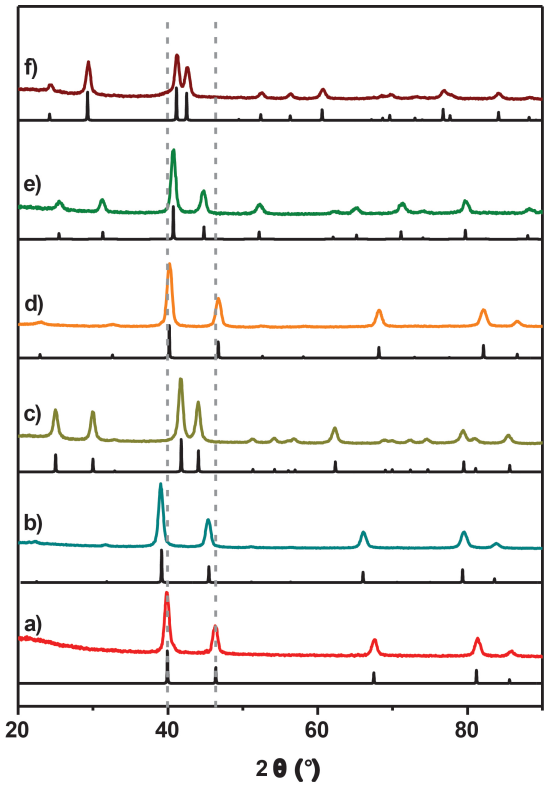

Figure 2: PXRD patterns for synthesized a) $Pt@mSiO_2$ and b-f) intermetallic $Pt_xM@mSiO_2$ NPs with Pt_xM being b) Pt_3Sn, c) PtSn, d) Pt_3Zn, e) PtZn, f) PtPb. For comparison are their simulated patterns (in black) obtained using available standard JCPDS data.

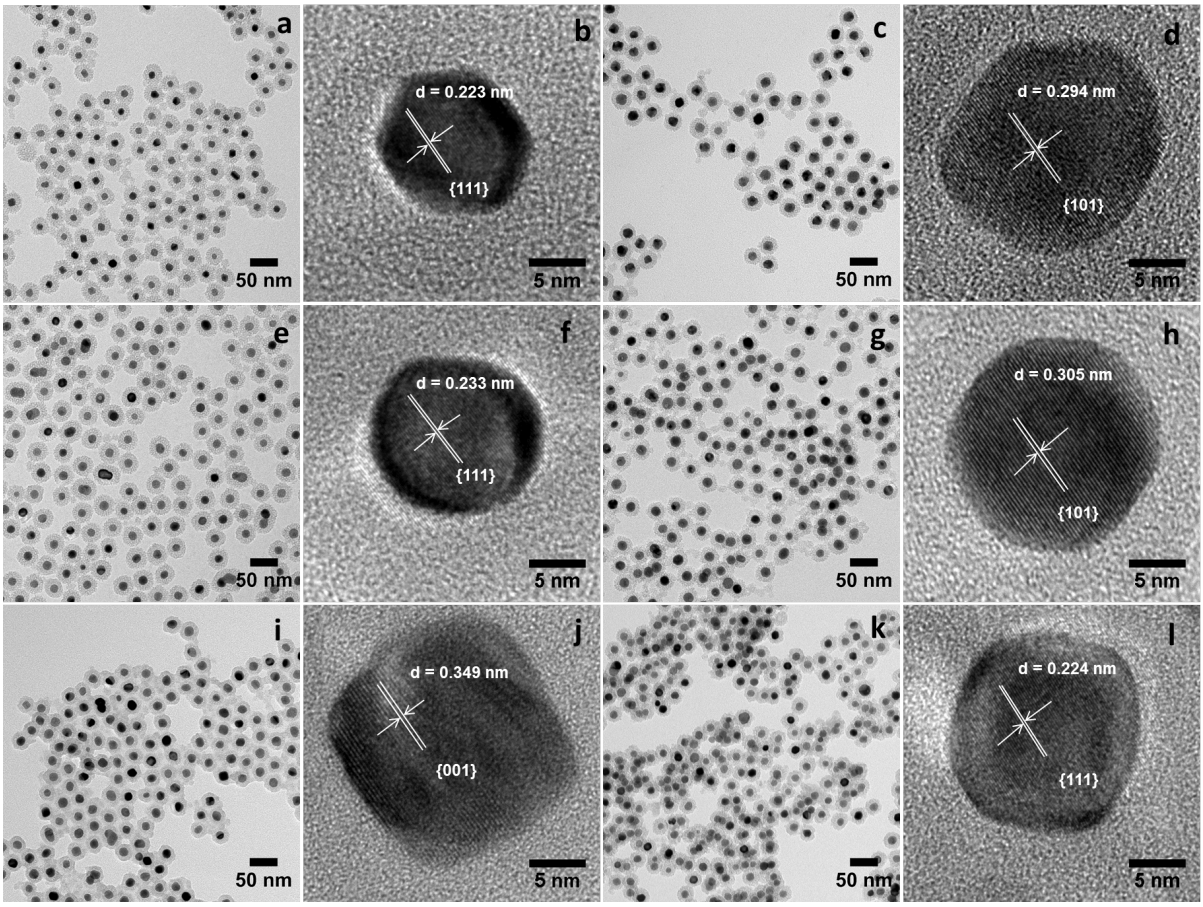

Figure 3: TEM and HRTEM images of a, b) Pt@mSiO$_2$ and c-l) intermetallic Pt$_x$M@mSiO$_2$ NPs with Pt$_x$M being c, d) PtSn; e, f) Pt$_3$Sn; g, h) PtPb; i, j) PtZn; and k, l) Pt$_3$Zn.

Comparing the overall size of the starting Pt@mSiO$_2$ NPs (36.1 ± 1.5 nm, Figure S2a) to those of the intermetallic compound NPs (Pt$_3$Sn@mSiO$_2$ = 36 ± 1.6 nm, PtSn@mSiO$_2$ = 35.8 ± 1.7, PtPb@mSiO$_2$ = 35.1± 1.8 nm, PtZn@mSiO$_2$ = 34.6 ± 1.3 nm, Pt$_3$Zn@mSiO$_2$ = 34.9 ± 1.6 nm, Figure S2d, g, j, m and p, respectively), the overall sizes of the particles (including the mSiO$_2$ shell) are almost unchanged. However, the sizes of the cores increase significantly (Fig S3e, h, k, n, and q for the nanoparticle cores of Pt$_3$Sn, PtSn, PtPb, PtZn, and Pt$_3$Zn, respectively), accompanied by a decrease in the thickness of the mesoporous silica shell (Figures S2f, i, l, o and r). These size increases in the cores observed from the TEM indicate the diffusion of the secondary metal precursors through the mSiO$_2$ shell and their reduction/deposition on the Pt core.

EDX line-scans carried out on single PtSn@mSiO$_2$ particles show that Pt and Sn were predominantly in the metallic core of the composite NPs (Figure S3 and S4). Table S1 summarizes the observed size increase in the metal core going from Pt to intermetallic NPs seen in TEM, which also agrees with the theoretical values calculated from the corresponding crystal lattice constants assuming no loss of Pt. The decrease in mSiO$_2$ shell thickness could be due to etching of less cross-linked internal silica under synthesis conditions. Park et al. reported the internal hollowing of silica spheres in aqueous media suggesting the relatively less cross-linked, high surface-energy inner environs to be more reactive and susceptible to dissolution, especially in aqueous or basic media.[36] Other reports have also suggested a preferential internal etching of silica rather than at the periphery.[37,38] N_2 physisorption measurements carried out on a sample of Pt@mSiO$_2$ and PtSn@mSiO$_2$ show the BET surface area decreases from 570 to 474 m^2/g after converting the core from Pt to PtSn, which agrees with the decrease in the mSiO$_2$ shell thickness (Figure S5 and Table S2). The pore size of the mesoporous SiO$_2$ shell increases slightly from 2.5 nm (Pt@mSiO$_2$) to 2.7 nm (PtSn@mSiO$_2$).

Catalysis. Furfural hydrogenation was carried out in a gas-phase plug-flow reactor equipped with an online gas chromatograph. Pt@mSiO$_2$ and PtSn@mSiO$_2$ were calcined at 500°C for 4h in air to remove organic residues from synthesis and reduced at 300°C for 4h under 10% H_2/He before catalysis studies. PtSn@mSiO$_2$ after this calcination and reduction treatment, as observed by TEM and measured by PXRD, is still well encapsulated within the silica shell and maintains its pure intermetallic phase (Figure S6). PtSn@mSiO$_2$ exhibits greatly improved conversion and selectivity in furfural hydrogenation to furfuryl alcohol compared with Pt@mSiO$_2$. Using PtSn@mSiO$_2$ containing the same amount of Pt as in Pt@mSiO$_2$, the conversion reaches 99% in the hydrogenation of furfural, while it is only 24% for Pt@mSiO$_2$ (Figure 4a). In

the case of PtSn@mSiO$_2$ high selectivity (97%) was also obtained towards furfuryl alcohol – the desired product. In contrast, Pt@mSiO$_2$ generated many decomposition products, such as furan, tetrahydrofuran, propane and butane (see Figure S7-9 for product distributions).

Along with the greatly enhanced furfuryl alcohol selectivity on PtSn@mSiO$_2$ compared to that on Pt@mSiO$_2$, the intermetallic catalyst is very stable, giving close to 100% conversion over a time on stream study for 40 hours. As the conversion is too high to evaluate the actual stability of PtSn@mSiO$_2$, we decreased the amount of the catalyst (0.26 mg of PtSn@mSiO$_2$, containing 0.124 mg Pt) to tune the furfural conversion to ~ 20%. Again, the catalyst is stable for a 40 hour-test after an initial induction period (Figure 4b). Moreover, the low conversion data on PtSn@mSiO$_2$ shows that only one-tenth the amount of Pt is needed in the intermetallic catalyst compared to the pure Pt catalyst to achieve similar conversion of furfural.

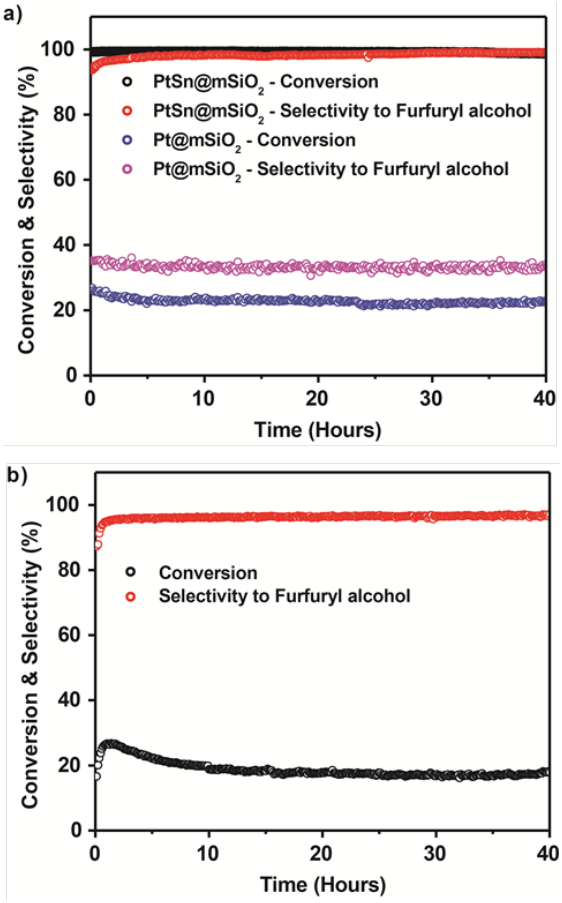

Figure 4: a) Catalytic performance of Pt@mSiO$_2$ versus PtSn@mSiO$_2$. Pt content (Pt mass = 1.26 mg) in both catalysts was kept fixed. b) Furfural hydrogenation by PtSn@mSiO$_2$ with a lower amount of the catalyst (0.26 mg, Pt mass = 0.124 mg). Reaction conditions for furfural hydrogenation: Furfural/H$_2$/He = 0.023/11.4/8.6 mL/min, 160°C.

This PtSn@mSiO$_2$ intermetallic catalyst demonstrates that greatly enhanced activity and selectivity in the hydrogenation of furfural to furfuryl alcohol can be achieved compared to pure Pt NPs with largely reduced usage of the precious metal. Intermetallic Pt$_3$Sn@mSiO$_2$, containing the same amount of Pt, also showed around 95% selectivity to furfuryl alcohol but deactivated over time (Figure S13). However, it deactivated much slower in comparison to the unannealed PtSn alloy (Pt:Sn ratio = 3:1). The other intermetallic catalysts, including PtZn, Pt$_3$Zn and PtPb were also tested (Figure S14). All of them showed high selectivity to furfuryl alcohol however their conversions were lower than PtSn@mSiO$_2$ and Pt$_3$Sn@mSiO$_2$ for the same quantity of Pt employed.

To indicate the importance of the mesoporous encapsulation, a control catalyst was also prepared by supporting the Pt colloidal NPs onto MCF-17 without the mSiO$_2$ coating and then converting it to PtSn/MCF-17, using the same synthetic conditions used to prepare PtSn@mSiO$_2$. The TEM images clearly depict aggregation for the final intermetallic compound on the support (Figure S15), as a result of which conversion using the same quantity of Pt was far lower (stabilized at 4% after an induction period) for PtSn/MCF-17, although the selectivity is similar at around 96% to furfuryl alcohol (Figure S16). Copper chromite, the industrial catalyst used for the hydrogenation of furfural, was also tested under our reaction conditions. High conversion and good selectivity are observed initially. However, the catalyst decays after 2 hours (Figure S17).

X-ray Photoelectron Spectroscopy (XPS) Studies. Focusing on the best catalyst for furfural hydrogenation to understand the importance of the surface for activity and stability, XPS studies were carried out on the intermetallic samples of PtSn@mSiO$_2$. Sn has been known to segregate to the surface readily upon exposure to air in PtSn bimetallics due to its greater affinity for oxygen.[39-42] In furfural hydrogenation the freshly reduced sample showed higher conversion and greater stability compared to the sample that had been exposed to air for two weeks (Figure S18), although their selectivities were similar (96-98%). From the XPS spectra (Figure S22), the surface concentration of Pt:Sn on the pre-reduced sample was almost 1:1 (Pt:Sn surface ratio = 1:1.1; Pt:Sn ICP-MS ratio = 1:1.02; Table S3), while the PtSn sample that had been exposed to air for two weeks had a lower surface concentration of Pt relative to Sn (Pt:Sn = 1:1.3; ICP-MS ratio = 1:1.02; Table S3). For the Sn spectra (Figure S22b), it is evident that the oxide component is greater in the sample that had not been reduced just before the reaction. This was further verified by initially running a freshly reduced catalyst for a short period, following which the catalyst was calcined. The conversion of furfural drops drastically from ~100% to ~30% after calcination (Figure S19). A quantity of the same sample was also calcined in air at 500°C and measured by XPS (Figure S23), wherein the Sn is completely oxidized and the concentration of Sn is 5.5 times higher than Pt on the surface (Table S3).

Furthermore XPS measurements were conducted on PtSn$_{1.1}$@mSiO$_2$ synthesized with excess Sn (Pt:Sn = 1:1.12 measured by ICP-MS) and freshly reduced at 300°C before XPS measurements. We found that this 10% increase in the bulk Sn composition induced a 40% increase in the surface Sn concentration of the PtSn NPs (Pt:Sn surface ratio by XPS = 1:1.4, Table S3), which may have been responsible for its rapid decay in activity during furfural hydrogenation (Figure S20a). This seemed to indicate that although adding Sn was beneficial to the performance of the catalyst via the formation of intermetallic PtSn, Sn added beyond the required amount, to form the intermetallic, accumulated on the surface (Table S3) and was detrimental to the stability of the catalyst.

We also tried to measure if there is any surface segregation of Pt or Sn on the PtSn@mSiO$_2$ using ambient pressure (AP)-XPS, in which 0.2 Torr H_2 was used to treat the intermetallic NPs under different temperatures. The atomic percentage of Pt and Sn, as well as their ratios to Si, could be found in Table S4. The atomic ratio of surface Pt to Sn (1:1.1) is consistent with the bulk ratio. Annealing PtSn@mSiO$_2$ in H_2 at elevated temperatures, the composition of Pt and Sn barely changes, suggesting there is no segregation of Pt or Sn in the PtSn core under these reduction conditions. The ratios of Pt and Sn to Si are rather small, consistent with the fact that PtSn nanoparticle is encapsulated in the SiO_2 shell. The ratios under these pre-treatment conditions did not change much, indicating that the PtSn core still stays in the SiO_2 shell after 500°C reduction.

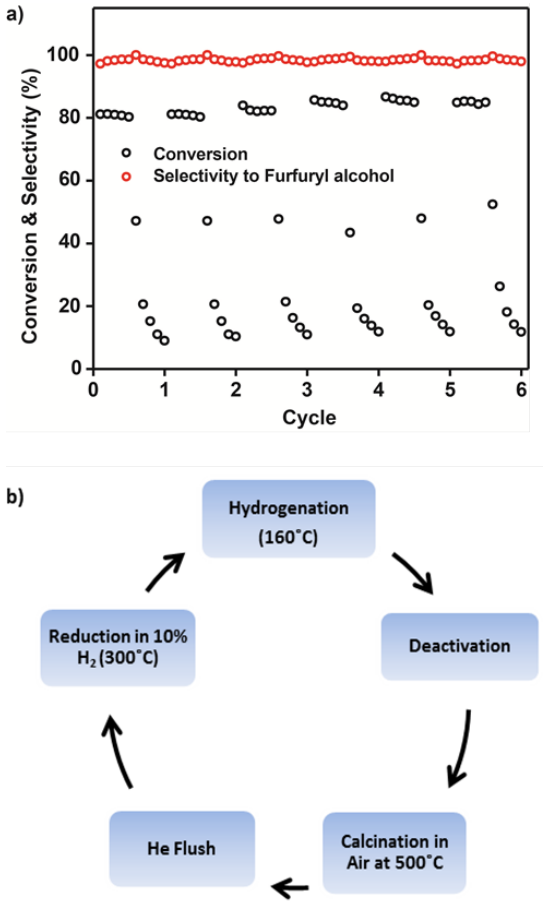

Figure 5: a) Regeneration cycles of PtSn@mSiO$_2$ in the hydrogenation of furfural; b) A schematic comprising all the steps in one regeneration cycle.

Catalyst Regeneration. A good measure of a catalyst's viability is the ease with which it can be conveniently regenerated after deactivation. A regeneration experiment was carried out to demonstrate the stability of the mSiO$_2$ protected intermetallic NPs. PtSn@mSiO$_2$ was first reduced at 300°C *in situ* in the flow system using 10% H_2, following which the hydrogenation of furfural was carried out for 35 minutes. Then the catalyst was deactivated intentionally by increasing the ratio of furfural to hydrogen. Following this deactivation the catalyst was calcined at 500 °C for 30 minutes in air to remove deposited carbon and then reduced at 300 °C for 30 minutes before the furfural hydrogenation in the next cycle. This constituted a single cycle. In total 6 cycles were carried out to demonstrate the ability to regenerate the catalyst (Figure 5). The conversion was tuned to 80% on purpose to show the activity of the catalysts is fully retained after each deactivation-regeneration cycle.

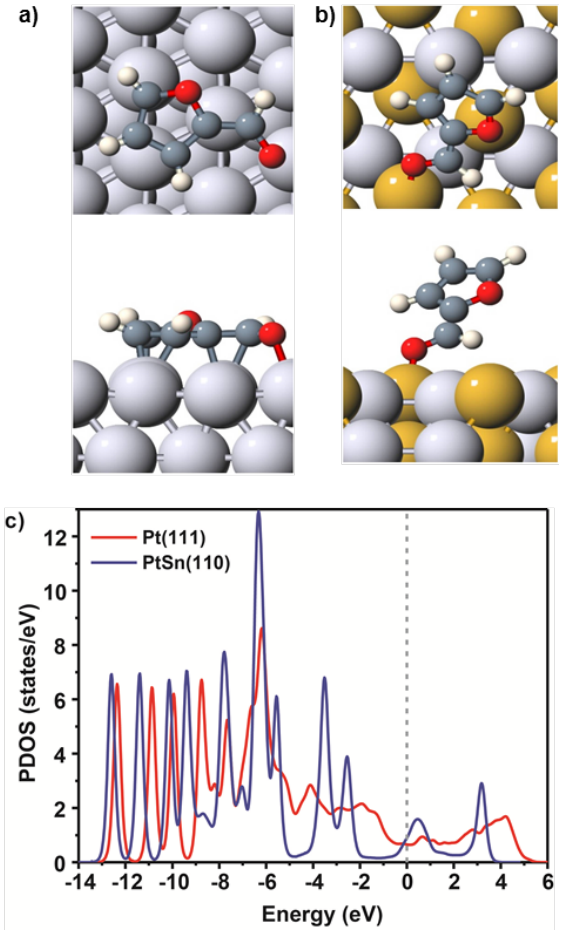

Figure 6. Most preferred adsorption configuration for furfural a) flat on Pt(111) and b) tilt on PtSn(110) surfaces with c) the corresponding projected density of states (PDOS). Large grey (brown) spheres are Pt (Sn) atoms in the surfaces; small gray, red and white spheres are C, O and H atoms in furfural. The top (bottom) panel is the top (side) view.

DFT Studies. To explain the improved hydrogenation selectivity toward furfuryl alcohol on the surface of intermetallic NPs, we performed DFT-PBE calculations to compare the adsorption of furfural on PtSn(110) and Pt(111) surfaces. We chose PtSn(110) surface for it has the lowest surface energy among the surfaces with exposed Pt atomic chains in the NiAs structure.[43] The most stable configurations of furfural on the two surfaces are shown in Figure 6a and b, with their corresponding projected density of states (PDOS) shown in (c). On Pt(111) the most preferred configuration is flat with the two

C=C bonds in the furan ring and the C=O bond sitting along three different Pt-Pt bridge sites, agreeing with other studies.[44,45] The adsorption energy is 0.87 eV. In contrast, on PtSn(110), the most preferred configuration is tilted with the O in C=O group sitting on top of Sn site. The adsorption energy is reduced significantly to 0.33 eV. This reduction is expected from our earlier study of CO adsorption on PtPb and PtBi surfaces[43] having the same NiAs structure, because the Pt *d*-band center on (110) is pushed toward lower energy and further away from the Fermi level due to the charge transfer from the *p*-metals.

The PtSn(110) surface can be characterized as Pt-Pt chains decorated with Sn to form Pt-Pt-Sn trimers locally. Even though Pt-Pt bridge sites are still available, which can accommodate the vertical adsorption of CO, the relatively larger furfural molecule does not have its C=C and C=O bond sit along these bridge sites (they are unstable) and become tilted after relaxation. From PDOS (Figure 6c), this is clearly shown by furfural on PtSn (111) retaining the molecular HOMO−1 (−3.5 eV), HOMO (−2.5 eV), LUMO (0.5 eV) and LUMO+1 (3.0 eV) states with part of the broadened LUMO-derived band shifted below the Fermi level and filled by charge transfer from Sn. In contrast, there is a strong band hybridization between furfural and Pt(111) in the flat configuration due to the direct C-Pt bonds. The tilt configuration on Cu(111) versus flat on Pt(111) has been used to explain[45] the high selectivity toward hydrogenation on Cu(111) because the channel for the activation of C-C is effectively closed. Similarly here, we think that the enhanced selectivity for furfural hydrogenation with PtSn intermetallic NPs is also due to its preferred tilted configuration on PtSn(110). Future study will investigate the reaction pathway and kinetic barriers, including other surface terminations of PtSn.

In conclusion, we have synthesized a series of monodisperse silica shell-encapsulated Pt-based intermetallic NPs, including PtSn, Pt_3Sn, PtPb, PtZn, and Pt_3Zn. As demonstrated in the hydrogenation of furfural, the PtSn@mSiO_2 (made with an optimum molar ratio of Pt:Sn = 1:1) intermetallic phase exhibited superior activity and selectivity to furfuryl alcohol in comparison to Pt@mSiO_2. The Pt atoms in the intermetallic compound benefit from an ordered environment, which is deemed responsible for the enhanced activity and selectivity in the hydrogenation of furfural to furfuryl alcohol. From XPS studies, a stoichiometric surface ratio of Pt and Sn is found to be the most optimum surface for the longevity of the catalyst. Using AP-XPS, we find the surface Pt to Sn ratio remains constant under reduction conditions. DFT calculations suggest the enhanced furfuryl alcohol selectivity in furfural hydrogenation on PtSn over Pt is correlated with the different adsorption configuration of furfural in these two systems. This work demonstrates that greatly enhanced activity and selectivity could be achieved using intermetallic nanoparticle catalysts, containing less precious metal. The mesoporous silica encapsulation could effectively prevent the aggregation of PtSn NPs during catalyst synthesis and regeneration. Using this *ship-in-a-bottle* strategy, intermetallic NPs with a broad spectrum of compositions could be conveniently synthesized, which will allow us to explore a plethora of opportunities in heterogeneous catalysis.

ASSOCIATED CONTENT

Supporting Information

Experimental details about the synthesis of intermetallic compounds, catalysis measurements, size distribution of NPs, nitrogen sorption, further XPS measurements can be found in the Supporting Information. This material is available free of charge via the Internet at http://pubs.acs.org.

AUTHOR INFORMATION

Corresponding Author

*whuang@iastate.edu

Author Contributions

The manuscript was written through contributions of all authors.

Notes

The authors declare no competing financial interest.

ACKNOWLEDGMENT

This research was supported by the Ames Laboratory Royalty Account and Iowa State University startup funds (R.V.M., C.X., T.W.G, J.G., Y.P., Z.Q., W.H.). Acknowledgment is also made to the Donors of the American Chemical Society Petroleum Research Fund for partial support of this research (R.V.M., C.X., T.W.G, J.G., Y.P., Z.Q., W.H.). This research at Ames Laboratory was partially supported by the U.S. Department of Energy (DOE), Office of Science, Basic Energy Sciences (BES), Materials Science and Engineering Division (L.-L.W. and D.D.J). The Ames Laboratory is operated for the U.S. DOE by Iowa State University under Contract No. DE-AC02-07CH11358. We thank Gordon J. Miller for use of his XRD and XPS, and Igor I. Slowing for use of his ICP-AES. We also thank Jim Anderegg for all the XPS measurements.

REFERENCES

(1) Studt, F.; Abild-Pedersen, F.; Bligaard, T.; Sørensen, R. Z.; Christensen, C. H.; Nørskov, J. K. *Science* **2008**, *320*, 1320.

(2) Xiao, C.; Wang, L.-L.; Maligal-Ganesh, R. V.; Smetana, V.; Walen, H.; Thiel, P. A.; Miller, G. J.; Johnson, D. D.; Huang, W. *J. Am. Chem. Soc.* **2013**, *135*, 9592.

(3) Studt, F.; Sharafutdinov, I.; Abild-Pedersen, F.; Elkjaer, C. F.; Hummelshoj, J. S.; Dahl, S.; Chorkendorff, I.; Norskov, J. K. *Nat. Chem.* **2014**, *6*, 320.

(4) Armbrrmbr; Sharafutdinov, I.; Abild-Pedersen, F.; Elkjaer, C. F.; Hummelshoj, J. S.; Dahl, S.; Chorkendorff, I.; Norskov, J. K. K. S, and Igor I. Slowing for use of his ICP-AES.fural to furfu*Nat. Mater.* **2012**, *11*, 690.

(5) Armbrrmbr. Sha; Schlögl, R.; Grin, Y. *Sci. Technol. Adv. Mater.* **2014**, *15*, 1.

(6) Armbrrmbrol. Adv. Mater. R.; Grin, Y. dersen, F.; Elkjaer, C. F.; Hummelshoj,*J. Am. Chem. Soc.* **2010**, *132*, 14745.

(7) Armbrrmbrm. Soc.. Mater. R.; Grin, Y. dersen, F.; Elkjaer, C. F.; HummR. *J. Am. Chem. Soc.* **2011**, *133*, 9112.

(8) Schaak, R. E.; Sra, A. K.; Leonard, B. M.; Cable, R. E.; Bauer, J. C.; Han, Y. F.; Means, J.; Teizer, W.; Vasquez, Y.; Funck, E. S. *J. Am. Chem. Soc.* **2005**, *127*, 3506.

(9) Leonard, B. M.; Bhuvanesh, N. S.; Schaak, R. E. *J. Am. Chem. Soc.* **2005**, *127*, 7326.

(10) Cable, R. E.; Schaak, R. E. *Chem. Mater.* **2005**, *17*, 6835.

(11) Sra, A. K.; Schaak, R. E. *J. Am. Chem. Soc.* **2004**, *126*, 6667.

(12) Leonard, B. M.; Schaak, R. E. *J. Am. Chem. Soc.* **2006**, *128*, 11475.

(13) Bauer, J. C.; Chen, X.; Liu, Q.; Phan, T.-H.; Schaak, R. E. *J. Mater. Chem.* **2008**, *18*, 275.

(14) Li, C.; Chen, Y.; Zhang, S.; Xu, S.; Zhou, J.; Wang, F.; Wei, M.; Evans, D. G.; Duan, X. *Chem. Mater.* **2013**, *25*, 3888.

(15) Schultz, M. J.; Zhang, X. Y.; Unarunotai, S.; Khang, D. Y.; Cao, Q.; Wang, C. J.; Lei, C. H.; MacLaren, S.; Soares, J.; Petrov, I.; Moore, J. S.; Rogers, J. A. *Proc. Natl. Acad. Sci. U. S. A.* **2008**, *105*, 7353.
(16) Zhang, T.; Zhao, H.; He, S.; Liu, K.; Liu, H.; Yin, Y.; Gao, C. *ACS Nano* **2014**, *8*, 7297.
(17) Huang, X.; Guo, C.; Zuo, J.; Zheng, N.; Stucky, G. D. *Small* **2009**, *5*, 361.
(18) Qiao, Z.-A.; Zhang, P.; Chai, S.-H.; Chi, M.; Veith, G. M.; Gallego, N. C.; Kidder, M.; Dai, S. *J. Am. Chem. Soc.* **2014**, *136*, 11260.
(19) Joo, S. H.; Park, J. Y.; Tsung, C.-K.; Yamada, Y.; Yang, P.; Somorjai, G. A. *Nat. Mater.* **2009**, *8*, 126.
(20) Feldmann, C. *Adv. Funct. Mater.* **2003**, *13*, 101.
(21) Kang, Y.; Pyo, J. B.; Ye, X.; Gordon, T. R.; Murray, C. B. *Acs Nano* **2012**, *6*, 5642.
(22) Lange, J.-P.; van der Heide, E.; van Buijtenen, J.; Price, R. *ChemSusChem* **2012**, *5*, 150.
(23) Yan, K.; Wu, G.; Lafleur, T.; Jarvis, C. *Renew. Sustainable Energy Rev.* **2014**, *38*, 663.
(24) G24)üG24). I.; Gallo, J. M. R.; Alonso, D. M.; Wettstein, S. G.; Lim, W. Y.; Dumesic, J. A. *Angew. Chem.-Int. Edit.* **2013**, *52*, 1270.
(25) Gonzalez Maldonado, G. M.; Assary, R. S.; Dumesic, J.; Curtiss, L. A. *Energy Environ. Sci.* **2012**, *5*, 6981.
(26) Zhang, Z.; Dong, K.; Zhao, Z. *ChemSusChem* **2011**, *4*, 112.
(27) Radhakrishnan, L.; Reboul, J.; Furukawa, S.; Srinivasu, P.; Kitagawa, S.; Yamauchi, Y. *Chem. Mater.* **2011**, *23*, 1225.
(28) Wang, H.; Yao, J. *Ind. Eng. Chem. Res.* **2006**, *45*, 6393.
(29) Liu, D.; Zemlyanov, D.; Wu, T.; Lobo-Lapidus, R. J.; Dumesic, J. A.; Miller, J. T.; Marshall, C. L. *J. Catal.* **2013**, *299*, 336.
(30) Pang, S. H.; Medlin, J. W. *ACS Catal.* **2011**, *1*, 1272.
(31) Pang, S. H.; Schoenbaum, C. A.; Schwartz, D. K.; Medlin, J. W. *Nat Commun* **2013**, *4*.
(32) Pang, S. H.; Schoenbaum, C. A.; Schwartz, D. K.; Medlin, J. W. *ACS Catal.* **2014**, *4*, 3123.
(33) Pushkarev, V. V.; Musselwhite, N.; An, K.; Alayoglu, S.; Somorjai, G. A. *Nano Lett.* **2012**, *12*, 5196.
(34) Baker, L. R.; Kennedy, G.; Van Spronsen, M.; Hervier, A.; Cai, X.; Chen, S.; Wang, L.-W.; Somorjai, G. A. *J. Am. Chem. Soc.* **2012**, *134*, 14208.
(35) KijeńKije J.; Winiarek, P.; Paryjczak, T.; Lewicki, A.; Mikołajska, A. *Appl. Catal. A-Gen.* **2002**, *233*, 171.
(36) Park, S.-J.; Kim, Y.-J.; Park, S.-J. *Langmuir* **2008**, *24*, 12134.
(37) Grzelczak, M.; Correa-Duarte, M. A.; Liz-Marz-MarzłajsK*Small* **2006**, *2*, 1174.
(38) Roca, M.; Haes, A. J. *J. Am. Chem. Soc.* **2008**, *130*, 14273.
(39) Yu, K.; Wu, Z.; Zhao, Q.; Li, B.; Xie, Y. *J. Phys. Chem. C* **2008**, *112*, 2244.
(40) Jugnet, Y.; Loffreda, D.; Dupont, C.; Delbecq, F.; Ehret, E.; Cadete Santos Aires, F. J.; Mun, B. S.; Aksoy Akgul, F.; Liu, Z. *J. Phys. Chem. Lett.* **2012**, *3*, 3707.
(41) Tao, F.; Zhang, S.; Nguyen, L.; Zhang, X. *Chem. Soc. Rev.* **2012**, *41*, 7980.
(42) Wang, X.; Stöver, J. r.; Zielasek, V.; Altmann, L.; Thiel, K.; Al-Shamery, K.; Bäumer, M.; Borchert, H.; Parisi, J. r.; Kolny-Olesiak, J. *Langmuir* **2011**, *27*, 11052.
(43) Wang, L. L.; Johnson, D. D. *J. Phys. Chem. C* **2008**, *112*, 8266.
(44) Liu, B.; Cheng, L.; Curtiss, L.; Greeley, J. *Surf. Sci.* **2014**, *622*, 51.
(45) Vorotnikov, V.; Mpourmpakis, G.; Vlachos, D. G. *ACS Catal.* **2012**, *2*, 2496.

Authors are required to submit a graphic entry for the Table of Contents (TOC) that, in conjunction with the manuscript title, should give the reader a representative idea of one of the following: A key structure, reaction, equation, concept, or theorem, etc., that is discussed in the manuscript. Consult the journal's Instructions for Authors for TOC graphic specifications.